Peer-reviewed version available at Minerals 2018, 8, 465; doi:10.3390/min8100465

Case Report

Multi-analytical investigation of stains on dimension stones in Master Valentim's Fountain, Brazil

Roberto Carlos da Conceição Ribeiro*, Patrícia Marques Ferreira de Figueiredo and Daniel Silva Barbutti.

Centre for Mineral Technology (CETEM), Av. Pedro Calmon 900, Cidade Universitária, Rio de Janeiro, Brazil.
* Correspondence: rcarlos@cetem.gov.br; Tel.: +55-21-3865-7264

Abstract: Master Valentim's fountain became an important historical patrimony for Brazil, being portrayed by famous artists among them Jean-Baptiste Debret. In 1938, it was registered as cultural heritage by the Brazilian National Historical and Artistic Heritage Institute (IPHAN), and in 1990 it was subjected to excavation and restoration works. The fountain was built in Gneiss and Lioz limestone, with metallic plates and mortar connecting the Gneiss blocks. Currently, deteriorations in the fountain stones can be observed such as light stains and some aesthetic modifications caused by inadequate restorations. Petrography, XRF, XRD, Physical Properties, Colorimetry, Electrical Conductivity, ICP-OES, SEM-EDX, and TGA were performed in order to characterize the Gneiss blocks, the metallic plates, the stones used in previous restorations, as well as light stains observed on the Gneiss blocks. The petrography and XRD analyses inferred that light stains may have been caused by the formation of an insoluble salt as a result of the association of the lead from the plates with other elements. The XRD analysis on the light staining area indicated presence of cerussite ($PbCO_3$), and anglesite ($PbSO_4$), which are the probable cause of the light stains. The SEM-EDX results suggested that sulfur is the main element associated to lead.

Keywords: Master Valentim's Fountain; Gneiss; Lioz limestone; Conservation and restoration.

1. Introduction

Currently, fountains are generally associated with aesthetic components. Nevertheless, they were initially built with the purpose of water supply sources. The fountain designed by Carlos Mardel is an example of this. It was inaugurated in 1747 at Terreiro do Paço in downtown Rio de Janeiro, Brazil (area known as Praça XV de Novembro nowadays) [1, 2]. In 1789, because of the distance from the sea, a new fountain was built closer to the port as a substitute of the original one. The artist responsible for the new fountain was called Valentim da Fonseca e Silva, better known as Master Valentim. The intention was to attend the demand from sailors and from the city, transforming the place into the main entrance door for travelers that arrived by means of ships [3]. At the beginning of the 20th century, after losing its usefulness as a water source, the fountain became an important monument which was recognized as cultural heritage by the Brazilian National Historical and Artistic Heritage Institute (IPHAN) in 1938. The fountain had its urban condition recovered in the 1990s, through a work of excavation and restoration that revealed the original staircase and berth [1].

The architecture of "Master Valentim's fountain" (Figure 1), as it is commonly called, was inspired by Rococo, the last phase of the Baroque period, that emerged in France in the mid-1700s [4]. The fountain was built in Gneiss and Lioz limestone [5]. To connect the Gneiss blocks and other blocks of the monument, Master Valentim applied his expertise in the manipulation of molten metals [6].

Peer-reviewed version available at Minerals 2018, 8, 465; doi:10.3390/min8100465

Figure 1. Master Valentim's fountain, located in Rio de Janeiro, Brazil.

The fountain can be seen in artistic productions of the famous French painter Jean-Baptiste Debret as shown in Figure 2. In this work of art, Debret portrayed Praça XV de Novembro, in the 19th century, and the Master Valentim's fountain can be seen in the background.

Figure 2. Debret's work of art named as "An afternoon at the Palace Square" (1826) [7].

Nowadays, it is possible to observe deteriorations in the fountain stones among them light stains on the Gneiss blocks, besides some inadequate aesthetic modifications.

Stone monuments located in open areas are vulnerable to physical, chemical, mechanical and biological weathering, that contribute to the alteration of their structural properties [8]. The in-depth knowledge of the mechanisms that promote such deteriorations is essential to provide adequate conservation and restoration actions of the dimension stones. Therefore, the aim of the present work is to investigate the light stains and other deteriorations observed on the fountain's dimension stones and their possible causes, as well as the results of previous restorations in comparison with the original materials used in the construction of this important monument.

2. Materials and Methods

The Gneiss blocks and the plates used to connect such blocks, the stones used in previous restorations, as well as light stains observed on the Gneiss blocks were evaluated. For this, the following analyses were performed: Petrography, X-ray fluorescence (XRF), X-ray diffraction (XRD), physical properties, colorimetry, electrical conductivity, inductively coupled plasma optical

Peer-reviewed version available at *Minerals* **2018**, *8*, 465; doi:10.3390/min8100465

emission spectrometry (ICP-OES), scanning electron microscopy-energy dispersive X-ray (SEM-EDX), and thermogravimetric analysis (TGA).

2.1. Petrography

Macroscopic and microscopic analyses were carried out on a fragment of a Gneiss block by means of an optical microscopy.

2.2. X-ray Fluorescence (XRF)

Chemical analyses through XRF were performed on areas where the Gneiss stones had light staining and in a connection plate of the monument that was provided for study.

For the connection plate, a benchtop PANalytical *Axios*^{mAX} 4.0 kW was used. The semi-quantitative *omnian* calibration standard was applied, with voltage and current ranges of 25-60 kV and 66-160 mA, respectively.

For the stains, the analyses were made in situ by means of a portable Bruker *S1 TURBO SD* spectrometer with a Silicon Drift Detector (SDD), maximum voltage 40 kV, and maximum anode current 60 μA (the maximum high-voltage available at 60 μA is 15 kV). The analyses were performed using the Universal mode, which is the default analysis type and works with automatic method detection and Dual Energy excitation.

2.3. X-ray Diffraction (XRD)

Mineralogical compositions of a fragment of a Gneiss block and a small portion of the light staining area collected at the site were evaluated. The XRD analyses were performed on a Bruker-AXS D4 Endeavor diffractometer, with Co kα radiation (40 kV, 40 mA). Diffraction patterns were acquired from 4 to 80 (2θ) at 0.02 steps. The identification of all minerals was done with Bruker-AXS's DIFFRAC.EVA suite.

2.4. Physical Properties

Tests were carried out, based on the ABNT NBR 15845-2, to evaluate the porosity and water absorption of the Gneiss fragment. Measurements were taken at atmospheric pressure by a *Marte* AD2000 hydrostatic balance.

2.5. Colorimetry

A portable BYK spectrophotometer (*Spectro-Guide Sphere Gloss*) was used to evaluate the color and gloss of the original stones and of those used in the restorations, as well as the stains mentioned previously. The colorimeter operates with 400-700 nm spectral range and 10 nm spectral resolution.

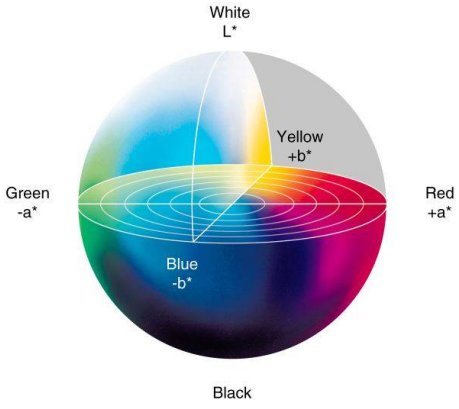

Figure 3. Representation of the CIELAB coordinates [9].

The results are expressed on CIELAB three-dimensional color space reference (Figure 3), where L* axis represents the lightness of a color, from the darkest black (L* = 0) to the brightest white (L* =

Peer-reviewed version available at Minerals 2018, 8, 465; doi:10.3390/min8100465

100); a* axis indicates greenness/redness of a color, from a* < 0 representing green, whereas a* > 0 denotes red; and b* axis expresses blue/yellow opponent colors, with negative values of b* for blue, and positive values of b* for yellow. Consequently, when the values of a* and b* are equal to zero the true neutral gray is expresses [9].

All colorimetric measurements for the original stones (used as control) and for altered or substitutes stones were performed in quadruplicates.

2.6. Electrical Conductivity

The conductivity tests were carried out with the Gneiss fragment. It was immersed in distilled water for approximately 120 hours. After, the water conductivity was analyzed with the assistance of TECNOPON portable equipment (model mCA-150P). For this, a standard solution of 146.9 μS/cm was used at a reference temperature of 25°C.

2.7. Inductively Coupled Plasma Optical Emission Spectrometry (ICP-OES)

ICP-OES was performed to quantify the possible elements present in the water that was analyzed by electrical conductivity. The following elements were quantified: sodium (Na), aluminum (Al), potassium (K), calcium (Ca), iron (Fe), magnesium (Mg), and sulfur (S). For such determination a Horiba Jobin Yvon *Ultima 2* spectrometer was used.

2.8. Scanning Electron Microscopy-Energy Dispersive X-ray (SEM-EDX)

The portion of the light staining area was also evaluated by means of SEM-EDX analyses. For this, a Hitachi TM3030Plus scanning electron microscope was used. The instrument was equipped with a Bruker X-Flash energy dispersive X-ray spectrometer with MIN SVE detector and scan generator connected.

2.9. Thermogravimetric Analysis (TGA)

TGA of the light staining, lead sulfate ($PbSO_4$), and lead carbonate ($PbCO_3$) samples was carried out for comparative purposes.

The analyses were performed using a NETZSCH thermogravimetric equipment, model STA 409 PC Luxx. Approximately 12 mg of the samples were weighed in an aluminum crucible and heated between 40 and 560 °C under a nitrogen atmosphere with a flow rate of 50 mL/min and a heating rate of 10 °C/min. The residue at 500 °C, the initial temperatures (T_{onset}), and the maximum temperatures (T_{max}) – at which the degradation rate was maximum – were determined through the mass loss *versus* temperature curves.

3. Results and Discussion

3.1. Dimension Stones Characterization

Macroscopically, the stone fragment sample is mesocratic, with a pinkish yellow color, medium to coarse grains, and light band characterized by the biotite segregation surrounding K-feldspar crystals. The sample showed signs of the weathering effects, which were identified on the K-feldspars through the color change to yellowish and the fragmented condition that facilitates their breakdown. It was possible to observe a rich matrix in biotite that is vulnerable to oxidation, and fracturing zones visible to the naked eye.

Microscopically, the sample is characterized by granoblastic and porphyroblastic textures, and medium to coarse, inequant grains, highlighting well-developed microcline and plagioclase crystals. The stone sample exhibited significantly alterations and microcracks, which are often occupied by recrystallized quartz grains (Figure 4). The mineralogical composition is mainly quartz, K-feldspar, plagioclase, and biotite. The accessory minerals are muscovite, gamet, and opaque minerals (≈ 1%). Sericite appears as an alteration mineral.

Peer-reviewed version available at Minerals 2018, 8, 465; doi:10.3390/min8100465

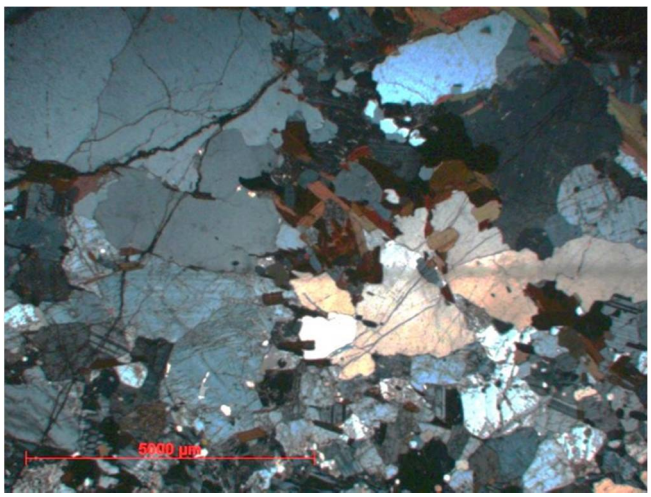

Figure 4. General Stone texture (crossed Nicols).

The quartz crystals are anhedral, with varied sizes, incipient microcracks, as well as plate and sutured boundaries with other minerals. Stretched and recrystallized crystals were observed surrounding the plagioclase and microcline minerals.

The K-feldspar crystals (microcline) are subhedral and anhedral, with varied sized (predominating larger sizes), and diffuse chess-board twinning due to the alteration.

The plagioclase crystals are subhedral and anhedral, with varied size, as well as Albite and Albite-Carlsbad twinning.

Both the K-feldspar and plagioclase crystals showed significantly alterations, with microcracks occupied by the sericite. Moreover, it was possible to observe quartz intergrowth in these minerals.

The biotite crystals are subhedral, with redish brown color, small size, and tabular shape. The crystals were disseminated throughout the slide and showed signs of deferrification due to the alteration.

The garnet crystals are subhedral and anhedral, exhibiting many microcracks.

According to the mineralogical composition and the macro and microscopic analyses, the stone sample could be classified as Augen Gneiss.

The XRD analysis indicated presence of quartz, plagioclase, K-feldspar, mica, zircon, and titatine. Such result is in agreement with the expected to Gneiss stones according to the literature [10].

The XRF analysis on the Gneiss stone areas without stains showed values around 7% of lead (Pb), 60% of silicon (Si) and 16% of aluminum (Al), with traces of other elements.

The electrical conductivity analysis performed in the water, in which the Gneiss fragment was immersed, indicated a value of 44.17 µS/cm at 25.7 °C, confirming the presence of ions. Table 1 shows the quantitative results of these ions determined by ICP-OES analysis.

Table 1. ICP-OES result.

Analytes	Na	Al	K	Ca	Fe	Mg	S
(mg.L^{-1})	2.1	< 0.007	0.81	3.5	0.01	0.43	< 0.01

Regarding the physical properties, porosity is one of the most important physical properties to evaluate the alterability of stones used in monuments, since this property is related to the stone's ability to absorb water (one of the most effective substances in stone weathering) [11]. The values of 1.0% and 0.4% are suggested as ideal for, respectively, porosity and water absorption of granites used as dimension stones [12]. The test performed on the Gneiss fragment indicated 3.36% and 1.45% for porosity and water absorption, respectively. These results demonstrate that the Gneiss blocks are in degradation process, since the values are higher than expected.

Peer-reviewed version available at Minerals 2018, 8, 465; doi:10.3390/min8100465

Colorimetric tests were performed to evaluate the replacement parts in previous restorations. It was easy to discern the original Gneiss stones from the replacement parts with the naked eye, since the latter were in better polishing state and with different colors (Figure 5). In the case of the restoration carried out on Lioz limestone balustrade and torches (Figure 6), although the difference was more subtle, it was still perceptible. Regarding the gloss, the new pieces exhibited an increase in the values, but without relevance.

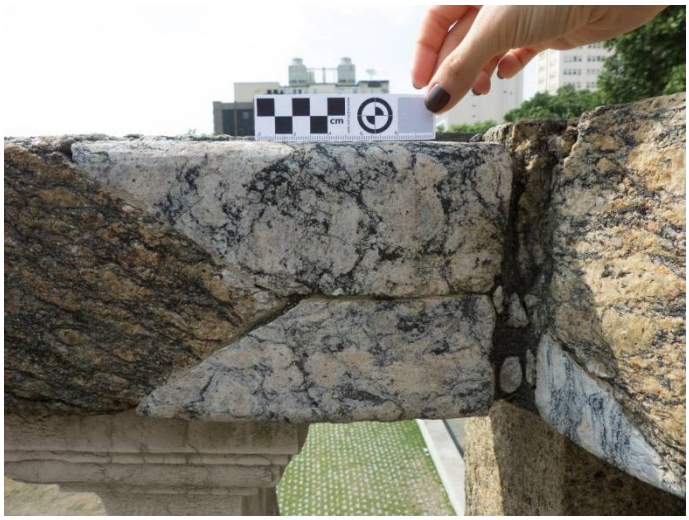

Figure 5. Substitute piece on a Gneiss block.

Figure 6. Lioz limestone area with restored part.

The analyses showed that Lioz limestone is light faded brown, slightly orange, possibly due to the weathering effects. Nevertheless, there is chromatic compatibility between the new parts and a sound Lioz limestone. On the other hand, Gneiss showed a tendency to brown, with a more intense orange. The substitute stones to the Gneiss showed grey color slightly orange.

For each surface analyzed, values were obtained for four points. Table 2 summarizes the examples of values obtained for one of these four points of some surfaces. The other values not shown in the table followed the same trends. However, it is important to note this is a monochromatic trend and therefore there is no direct relationship between the obtained color and the color saw with the naked eye, since the stone are heterochromatic.

Table 2. LAB parameters for the analyzed samples.

Samples	Altered/Substitute Stone Parameters				Standard Stone Parameters			
	L*	a*	b*	G	L*	a*	b*	G
Substitute Gneiss (torch top)	67.5	2.05	7.77	1.30	61.4	3.62	16.0	0.70
Substitute Gneiss (torch basis)	72.1	1.99	9.29	1.10	61.4	3.62	16.0	0.70
Substitute Gneiss (parapet)	65.7	0.42	5.94	1.00	55.3	5.07	15.3	0.50
Original Gneiss (external wall, light staining)	56.8	0.22	4.83	0.50	57.4	1.43	12.9	0.80
Lioz limestone (torch)	74.3	1.77	6.98	1.50	73.4	1.99	8.44	0.80
Lioz limestone (banister)	76.1	1.86	7.74	0.90	73.9	2.54	9.80	1.10

3.2. Plate Characterization

XRF analyses were performed at three different points on the connection plate (Figure 7) and the results indicated lead (Pb) as the major element. Such result was expected, since Pb was widely used by Master Valentim in his works. Furthermore, smaller levels of aluminum (Al) and silicon (Si) were verified, as well as traces of other elements. The values derived from the analyses ranged from 77.8 to 88.9% for lead oxide (PbO), 4.4 to 10.0% for silicon oxide (SiO_2) and 1.9 to 3.7% for aluminum oxide (Al_2O_3).

Figure 7. Lead plate used to connect the stone blocks of the monument.

3.3. Light Stains Characterization

The XRF analysis performed on the light stains (Figure 8) indicated high content of lead (Pb) and silicon (Si).

Figure 8. Light staining area on a Gneiss block.

Peer-reviewed version available at Minerals 2018, 8, 465; doi:10.3390/min8100465

The levels observed were approximately 50% of Pb, 38% of Si and 8% of Al, besides other elements. These results suggest that these stains may have been originated from the association of the lead of the plates used to connect the blocks with other elements such as sulfur (from the pollution present in the environment of high urban movement), forming an insoluble salt of white coloration.

The XRD analysis demonstrated presence of quartz, plagioclase, K-feldspar, and mica as expected for Gneiss stones. However, such analysis also showed peaks of cerussite ($PbCO_3$), and anglesite ($PbSO_4$), which are the probable cause of the light stains, as well as insignificant peaks of cotunnite ($PbCl_2$).

Figure 9 shows the SEM image zoom of staining area of the analyzed samples. The SEM-EDX results identified peaks of chlorine (Cl), potassium (K), carbon (C), sulfur (S), calcium (Ca), oxygen (O), iron (Fe), sodium (Na), magnesium (Mg), silicon (Si), and lead (Pb). Quantitative analysis indicated about 65% of Pb. In order to verify the possible elements related to Pb in the light staining area analyzed, elemental mapping of Pb, S, C and Si were performed as verified in Figure 10.

Figure 9. SEM image zoom of the staining area.

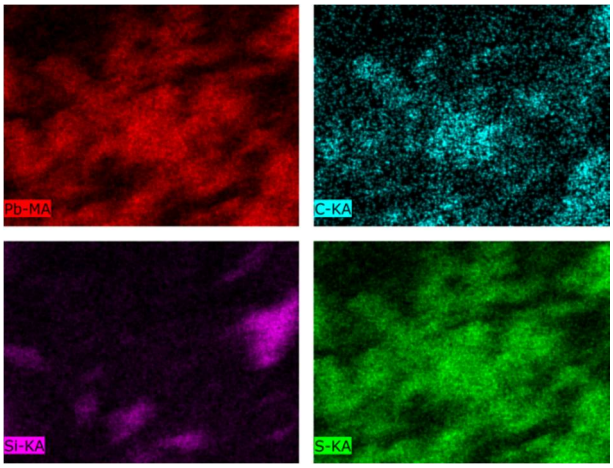

Figure 10. Elemental mapping of Pb, C, Si, and S individually.

Such results suggest that sulfur is the main element associated to lead. It is also possible to observe association between Pb and C, but occurring to a lesser extent when compared to S.

The results of ATG (Figure 11) indicated that the sample concerning change in the fountain is related to $PbSO_4$ formation since the thermal degradation curve is similar to this pure salt. Thus, it was believed that the sulfur pollution emanating from the vehicles was deposited on the surface of

Peer-reviewed version available at Minerals 2018, 8, 465; doi:10.3390/min8100465

the fountain and that this element was associated with the lead used as a grout, forming the stable salt of lead sulphate.

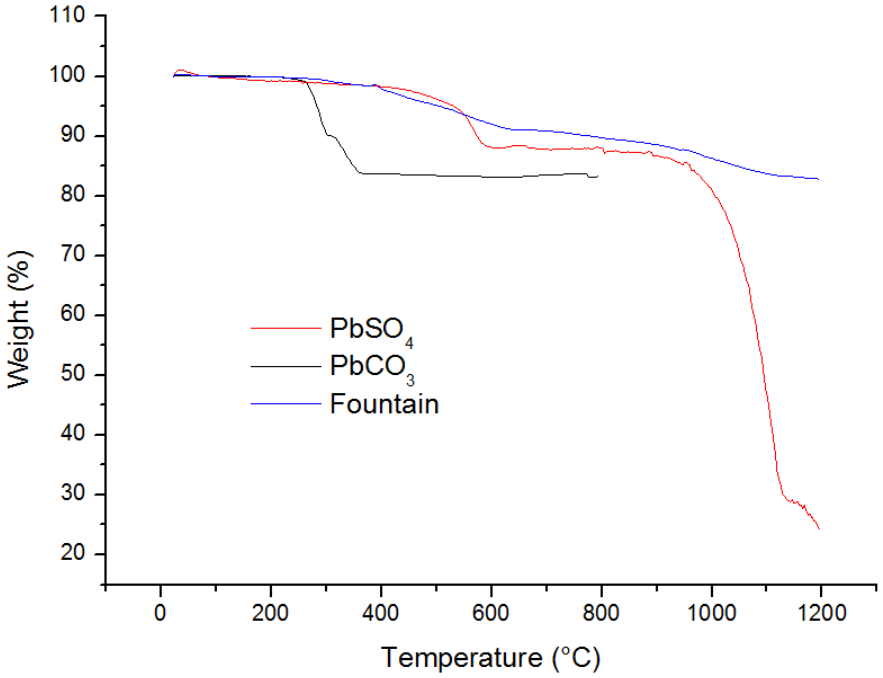

Figure 11: Thermal degradation curve showing the losses in each step with a rate of 10°C /min.

4. Conclusions

The petrographic analysis allowed classifying the stone sample as Augen Gneiss. Such sample showed microcracks and significantly alterations that are possibly related to weathering effects.

XRD analysis on the fragment of the Gneiss blocks identified minerals compatible with the expected to Gneiss stones (quartz, plagioclase, K-feldspar, mica, zircon, and titanite). However, for the light staining area this analysis also indicated presence of cerussite ($PbCO_3$) and anglesite ($PbSO_4$). Moreover, XRF analysis on the staining area demonstrated higher content of lead (Pb) than the one performed on Gneiss stone area without stains. These results suggest that the light stains may have been caused by the association of the lead in the connection plates (confirmed by XRF analysis) with other elements (sulfur or carbon), forming an insoluble salt of white coloration. SEM-EDX investigation confirmed presence of lead, sulfur and carbon on the light staining area. Elemental mapping suggested that sulfur is the main element associated to lead. Therefore, it is possible that the light stains are $PbSO_4$. The sulfur pollution emanating from the vehicles was deposited on the surface of the fountain and that this element was associated with the lead used as a grout, forming the stable salt of lead sulphate.

Regarding the previous restorations, the colorimetric evaluations showed differences in the chromatic trends between the Gneiss stones used in the restoration and the original ones. For Lioz limestone parts, the differences are more subtle but still noticeable to the naked eye. These observations point to the importance of prior technological support for the conservation and restoration of cultural heritages in order to minimize the likelihood of inadequate results.

Author Contributions: Conceptualization and Methodology, R.C.C.R.; Formal Analysis, P.M.F.F. and D.S.B.; Results interpretation, R.C.C.R. and P.M.F.F.; Writing-Original Draft Preparation, P.M.F.F.; Writing-Review, D.S.B.

Acknowledgments: The authors acknowledge the Centre for Mineral Technology (CETEM) for its infrastructure support and to the Brazilian National Council for Scientific and Technological Development (CNPq) for its financial support.

Conflicts of Interest: The authors declare no conflict of interest.

References

1. ARQGUIARio. Available online: http://arqguia.com/obra/chafariz-do-mestre-valentim/?lang=en (accessed on 12 June 2018).
2. Rio de Janeiro Aqui. Available online: http://www.riodejaneiroaqui.com/pt/chafariz-da-piramide.html (accessed on 12 June 2018).
3. IPHAN. Available online: http://portal.iphan.gov.br/ans.net/tema_consulta.asp?Linha=tc_hist.gif&Cod=2974 (accessed on 12 June 2018).
4. Thought Co. Available online: https://www.thoughtco.com/rococo-art-architecture-4147980 (accessed on 12 June 2018).
5. Telles, A. C. S. Atlas dos Monumentos Históricos e Artísticos do Brasil. Publisher: Brazil, 2007; pp. 138-139. Available online: http://portal.iphan.gov.br/uploads/publicacao/ColObrRef_AtlasMonumentosHistoricosArtisticosBrasil.pdf (accessed on 12 June 2018).
6. Brusadin, L.; Quites, M. A técnica da escultura em madeira com máscara de chumbo policromada: a contingência dos Cristos da Paixão da Ordem Terceira do Carmo de Outro Preto (MG). Visualidades 2016, 14 (1), 188-215, DOI 10.5216/vis.v14i1.35014.
7. Debret's Rio de Janeiro Castro Maya Collection. Rio de Janeiro, Brazil, 2015.
8. Öztrürk, I. Alkoxysilanes consolidation of stone and earthen building materials. Master's Thesis. University of Pennsylvania, Philadelphia, 1992.
9. Nazdar Ink Technologies. Available online: https://www.nazdar.com/en-us/News-events/ArtMID/4165/ArticleID/224 (accessed on 12 June 2018).
10. Marques, E. A. G.; Barroso, E. V.; Menezes Filho, A. P.; Vargas Jr., E. A. Weathering zones on metamorphic rocks from Rio de Janeiro – Physical, mineralogical and geomechanical characterization. Engineering Geology. 2010, 111, 1-18, DOI 10.1016/j.enggeo.2009.11.001.
11. National Research Council. Conservation of Historic Stone Buildings and Monuments. Washington, DC: The National Academies Press. DOI 10.17226/514.
12. Frazão, E. B.; Farjallat, J. E. Características tecnológicas das principais rochas silicáticas brasileiras usadas como pedras de revestimento. In I Congresso Internacional de Pedra Natural, Lisboa, Portugal, 1995, pp. 47-58.